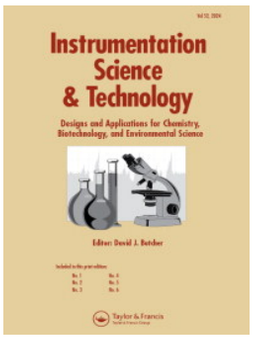

Instrumentation Science & Technology

ISSN: 1073-9149 (Print) 1525-6030 (Online) Journal homepage: www.tandfonline.com/journals/list20

Determination of carcinoembryonic antigen (CEA) by surface plasmon resonance-enhanced total internal reflection ellipsometry (SPRe-TIRE)

Aslı Erkal-Aytemur, Samet Şahin, Zafer Üstündağ, İbrahim Ender Mülazımoğlu & Mustafa Oguzhan Caglayan

To cite this article: Aslı Erkal-Aytemur, Samet Şahin, Zafer Üstündağ, İbrahim Ender Mülazımoğlu & Mustafa Oguzhan Caglayan (2024) Determination of carcinoembryonic antigen (CEA) by surface plasmon resonance-enhanced total internal reflection ellipsometry (SPRe-TIRE), Instrumentation Science & Technology, 52:2, 203-219, DOI: 10.1080/10739149.2023.2242921

To link to this article: https://doi.org/10.1080/10739149.2023.2242921

INSTRUMENTATION SCIENCE & TECHNOLOGY
2024, VOL. 52, NO. 2, 203–219
https://doi.org/10.1080/10739149.2023.2242921

Taylor & Francis
Taylor & Francis Group

Determination of carcinoembryonic antigen (CEA) by surface plasmon resonance-enhanced total internal reflection ellipsometry (SPRe-TIRE)

Aslı Erkal-Aytemur[a], Samet Şahin[b], Zafer Üstündağ[c], İbrahim Ender Mülazımoğlu[d], and Mustafa Oguzhan Caglayan[b]

[a]Rafet Kayış Faculty of Engineering, Fundamental Science, Alanya Alaaddin Keykubat University, Antalya, Turkey; [b]Faculty of Engineering, Department of Bioengineering, Bilecik Şeyh Edebali University, Bilecik, Turkey; [c]Faculty of Arts and Science, Department of Chemistry, Kütahya Dumlupınar University, Kütahya, Turkey; [d]Ahmet Keleşoğlu Faculty of Education, Chemistry Department, Necmettin Erbakan University, Konya, Turkey

ABSTRACT

A surface plasmon resonance-enhanced total internal reflection ellipsometric (SPRe-TIRE) aptasensor is reported for the determination of the carcinoembryonic antigen (CEA). A gold nanofilm-coated SF10 glass slide was modified with electrochemical diazonium salt reduction and gold nanoparticles (AuNPs) to form a sensor. Next, a specific aptamer for CEA was immobilized on the AuNPs via self-assembly. The platform was characterized by X-ray photoelectron spectroscopy, ellipsometry, and cyclic voltammetry for each step of the preparation of the sensor. CEA aptamers with different affinities were used. SPRe-TIRE employed total internal reflection geometry and AuNPs to enhance plasmon resonance for the sensitive and selective determination of CEA in human serum. The working range of the aptasensor was from 0.01 to 500 ng/mL with an optimum detection limit of 0.1 pg/mL.

KEYWORDS

Carcinoembryonic antigen (CEA); surface plasmon resonance-enhanced total internal reflection ellipsometry (SPRe-TIRE); aptasensor; cyclic voltammetry (CV)

Introduction

Cancer is an important disease that threatens human health globally and early detection plays a crucial role.[1] Cancer biomarkers are characteristic measures to indicate the risk and occurrence of cancer and patient outcome.[2] If cancer is detected, diagnosed and treated at an early stage, then the chances of survival significantly increase.[3] Carcinoembryonic antigen (CEA) is a glycoprotein and one of the well-known biomarkers for the diagnosis of liver, colon, breast, and colorectal cancer.[4–6]

CONTACT İbrahim Ender Mülazımoğlu mulazimoglu@gmail.com Ahmet Keleşoğlu Faculty of Education, Chemistry Department, Necmettin Erbakan University, Konya, Turkey; Mustafa Oguzhan Caglayan mocaglayan@gmail.com Faculty of Engineering, Department of Bioengineering, Bilecik Şeyh Edebali University, Bilecik, Turkey.

Supplemental data for this article can be accessed online at https://doi.org/10.1080/10739149.2023.2242921.

Although different serum cutoff CEA levels have been reported in the literature, a cancer-related condition is suspected when serum levels are higher than 5–10 ng/mL.[7] Therefore, the concentration of CEA in human serum is of great importance for cancer diagnosis.[8] In particular, the sensitive determination of CEA is crucial for early detection of disease onset or recurrence.[9] There are many immunoassay studies that include radiometric sensors,[10,11] enzymatic sensors,[12,13] fluoro-immunoassays,[14] piezoelectric immunosensors,[15] and electrochemical immunosensors[16] for CEA detection. However, the most immunoassays have disadvantages including long assay times and the use of complex techniques.[9,17] Therefore, a focus has been the development of rapid, sensitive, selective, and cost-effective methods for CEA that include colorimetric, electrochemical, surface plasmonic, fluorescence, chemiluminescence, and electrochemiluminescence biosensors.[5,18] However, some of these techniques require time-consuming steps, provide low sensitivity and selectivity, and need additional labeling to determine CEA.

An alternative diagnostic element to improve analytical selectivity and sensitivity is aptamers[19,20] that are single-stranded DNA or RNA oligonucleotides selected from a random or homologous library and been developed for various analytes since their first reports in 1994.[21,22] They are versatile recognition elements since they interact with the target showing as good affinity as the antibody-antigen interactions.[23] Aptamers also have advantages over antibodies such as stability, low cost, and ease of production.[24] Aptamers have been developed for the selective determination of CEA in various media with good sensitivity and selectivity, high accuracy, fast response, and low cost.[25–28]

In bio-related studies, thickness or ellipsometric functions (Δ, Delta, and Ψ, Psi) may be used for acquiring data related to changes on the sensor surface.[29] These ellipsometric functions obtained from the surface may be measured very accurately, within $< \pm 0.001$ degree, to define the characteristics of the surface.[30] The phase shift (Δ) is sensitive to the dielectric function of the materials deposited on the surface.[31] This sensitivity may be further enhanced using either internal reflectometry, plasmon resonance coupling, or both.[32] To enhance the signal *via* total internal reflection ellipsometry (TIRE), a Kretschmann configuration for total internal reflection is used with a thin gold layer for plasmon resonance.[33] When the resonance condition is fulfilled, the phase shift (Δ) becomes more sensitive to surface interactions where a recognition element and its analyte interact. These plasmon resonance conditions may be further altered using AuNPs.[34]

Herein, an SPRe-TIRE aptasensor was employed for the first time to determine CEA in buffer and human serum. For this purpose, two

previously described anti-CEA aptamers with different affinities and sequences (dissociation constant (K_d) of ~37.8 and 3.9 nM, respectively) were used.[35] Ellipsometry, as a sensitive method, uses both the phase difference (Δ, Delta) and the intensity (Ψ, Psi) differences of polarized monochromatic light reflected from surfaces. By definition, these ellipsometric values are the dielectric functions of a surface and are a function of the refractive indices and thicknesses of the thin layers of media where the incident light is reflected.[36] Ellipsometry is a powerful tool to examine the dielectric functions and thicknesses of various nanofilms produced in physics and materials laboratories.[37] On the other hand, employing this powerful tool in bio-related areas is still developing but several studies have been published using this strategy.[38–43]

An AuNP layer within the close vicinity of the plasmonic surface was employed to further enhance the signal using electrochemical diazonium salt reduction and SH–AuNPs interaction. Using the advantages of ellipsometry and plasmon resonance, we report for the first time a sensitive and selective CEA aptasensor based upon the SPRe-TIRE platform.

Experimental

All chemicals used in this study were of analytical purity and supplied by local representatives unless otherwise stated. Ultrapure water was used for cleaning purposes and in aqueous solution preparations (UPW, 18.2 MΩ cm, Human Power 1+, South Korea). The ellipsometer (Optosense, Turkey) has a TIRE setup and a flow cell for real-time measurements was used. The ellipsometer was also employed in the measurement of layer thicknesses and sensor responses without flow-cell (TIRE) arrangement. Thickness measurements were made using the built-in layer modeling tool of the ellipsometer using glass slide/metal layer and organic layer dielectric data. All results are the arithmetical means and standard deviations of at least 5 repetitions unless stated otherwise.

Preparation of the gold-coated glass slides

A schematic of the CEA sensor platform is shown in Scheme 1. The gold-coated glass slides were prepared as follows. The 2.5 cm × 2.5 cm cut SF10 glass was cleaned in a 1:3 nitric acid/water boiling solution for 30 min to remove organic contaminants and oil. Next, the surface was prepared for metal coating by treatment with an oxygen plasma for 30 min in a chamber.[44] 3 nm chrome (Cr) was coated as an adhesive layer on the surface of the SF10 glass in a physical vapor deposition (PVD, Nanovak, Turkey) system. Lastly, 32 nm Au was coated to achieve plasmon resonance under a

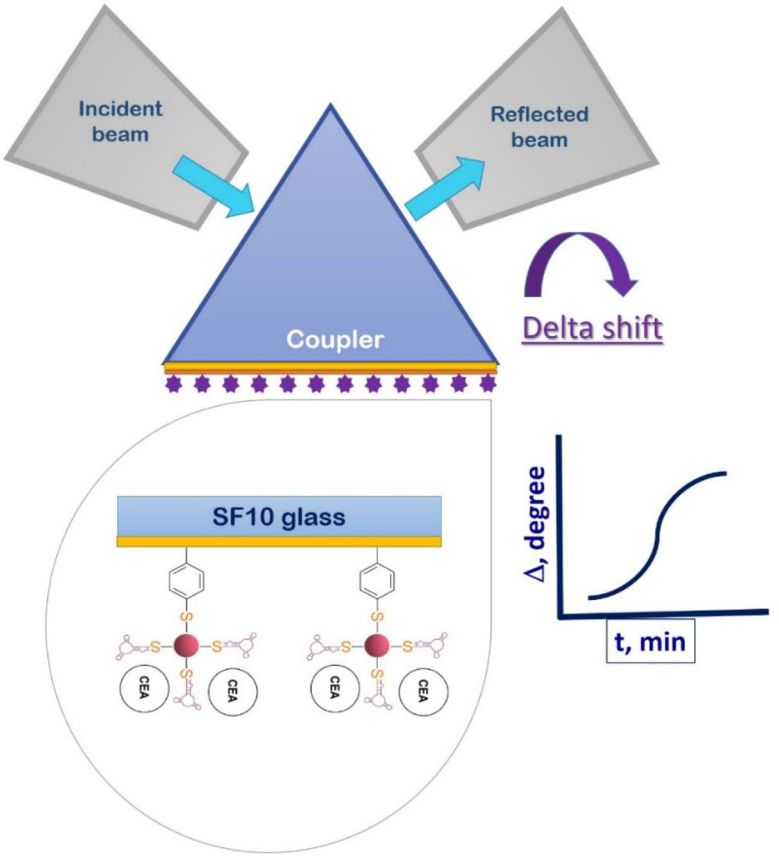

Scheme 1. Schematic of the sensor platform.

532 nm green laser at a 63° angle of incidence. This coated surface is abbreviated as SF10/Cr/Au.

Covalent bonding of the mercaptophenyl nanofilm on SF10/Cr/Au

The 4-mercaptobenzene diazonium salt (4MB-DAS) was prepared from the 4-aminothiophenol (4ATP, 4-mercaptoaniline, 125.2 g/mol) in the aqueous media using the procedure of Morita et al.[45] Briefly, 100 mg of 4ATP were dissolved in 20 mL of 0.5 M HCl and the temperature was maintained at 0 °C by cooling in an ice bath. 221 mg of $NaNO_2$ (69 g/mol) were dissolved in 2 mL of water and cooled. Next, the $NaNO_2$ solution was added dropwise into the continuously stirred 4ATP solution until gas formation was complete. The 4MB-DAS solution was kept in an ice bath so that the temperature of the mixture did not exceed 4 °C.

The SF10/Cr/Au was electrochemically modified by immersion in a 4MB-DAS solution. An SF10/Cr/Au electrode was used as the working electrode. A Ag/AgCl/KCl (saturated) was used as the reference electrode

and Pt wire as the counter electrode. Electrochemical modifications were done using the Reference-300 (Gamry, USA) electroanalyzer. The 4-mercaptophenyl nanofilm (4MP) was prepared on SF10/Cr/Au electrode by covalent bonding because of the electrochemical reduction of 4MB-DAS. The produced sensor was designated to be the SF10/Cr/Au/4MP. Nanofilm formation was characterized by cyclic voltammetry (CV) and impedance spectroscopy.

SF10/Cr/Au/4MP surface attachment of AuNPs, and aptamer immobilization

Au nanoparticle (AuNPs) synthesis was done according to the literature by a colloidal method.[46] 25 mL of 1.0 mM auric acid were treated with 2.5 mL of 1% $Na_3C_6H_5O_7{\cdot}2H_2O$ added dropwise to the boiling solution. After the formation of AuNPs, which was determined to be complete as a result of the color change, the well-mixed mixture was cooled.[47] The colloidal solution was centrifuged at 15,000 rpm for 10 min and washed three times sequentially with deionized water and ethanol.

The synthesized AuNPs were attached to the SF10/Cr/Au/4MP surface through a SH–Au bond. Aptamers pre-modified with SH and C_6H_{12} from the 5′ terminus as shown in Table 1 and different concentrations in phosphate-buffered saline (PBS, pH 7.4) were immobilized on the AuNP surface.[35,48] As a result of monitoring the simultaneous immobilization with SPRe-TIRE, both the immobilization time and the appropriate aptamer concentrations were optimized separately. In order to minimize unspecific interactions, mercaptohexanol (SH-C_6H_{12}-OH) in PBS was bound to the aptamer immobilized AuNPs surface using the incubation time and concentration specified in the literature.[49]

SPRe-TIRE measurements

In the ellipsometry measurements, the total internal reflection Kretschmann configuration for SPR coupling was preferred. All measurements were performed using 532 nm monochromatic light on the surface prepared with Au coating of appropriate thickness for SPR. The

Table 1. Anti-CEA aptamers employed in this study.

Aptamer	Sequences (from 5' to 3')	Dissociation constant (nM)	References
AntiCEA1	GGGG CGAC GTTG AGAT TCCG CTTG TGTA TTAG TAGT CCCC	37.8	[35]
AntiCEA2	ATAC CAGC TTAT TCAA TTGG GGTA GGGG GCGA AGCG ATAC CCTA ATCA GC	3.9	[48]

measurement interval depends on the time for the device to determine the Δ and ψ values according to the nulling procedure and was a maximum of 5 s. The flow cell had a volume of 50 µL and the flow rate was 3 µL/s. Only Δ values were measured at room temperature on the platform which resembles an SPR flow cell. The buffer solution was injected into the system with the modified and aptamer immobilized sensor chip. The Δ value obtained at this stage was considered to be the background, and the sensor response was calculated as the difference.

Interference and serum analysis

Interference studies of the aptamer sensors were carried out in PBS using possible interferences. All interferents used in this study were added in 10-fold excess of the CEA analyte (50 ng/mL and 500 ng/mL). The investigated interferences were α-fetoprotein (AFP), cancer antigen 125 (CA 125), and vascular endothelial growth factor (VEGF-165). In addition, CEA was spiked into commercial human serum samples (Sigma-Aldrich H4522, USA) and determined to characterize the potential for practical analysis.

X-ray photoelectron spectroscopy (XPS) characterizations

XPS spectra of C 1s and S 2p core levels of SF10/Cr/Au/4MP surfaces were obtained using a PHI 5000 Versa Probe spectrometer (ULVAC-PHI.) equipped with monochromatic Al K_α radiation (1486.6 eV).

Results and discussion

A 4MP nanofilm on the Au-coated slide was formed by a 3-cycled electrochemical reduction of 4MB-DAS. Figure 1 shows the alternating 3-cycle voltammogram of 4MB-DAS upon the SF10/Cr/Au electrode. In the first cycle, the irreversible peak current of the 4MB-DAS decreased showing that almost the entire surface was covered. With the last cycle, the peak current reached a steady state, which implies the formation of a modified surface.[50]

For each sample, ψ and Δ measurements were made from 10 points with 5 repetitions to determine the layer thickness using the ellipsometric model. A five-layer model was applied to air/organic layer/Au film/Cr film/substrate (SF10) to investigate the effect of the number of modification cycles upon the layer formation. The model parameters for the SF10 glass substrate, Cr layer, Au layer, and the 4MP organic layer were $n = 1.73793$; $n = 3.0390$ and $k = 3.330$; $n = 0.4137$ and $k = 2.4083$; and $n = 1.4600$. The obtained thickness values are listed in Table 2. After the first cycle, the thickness increased to around 1.2 nm. The thickness reached approximate

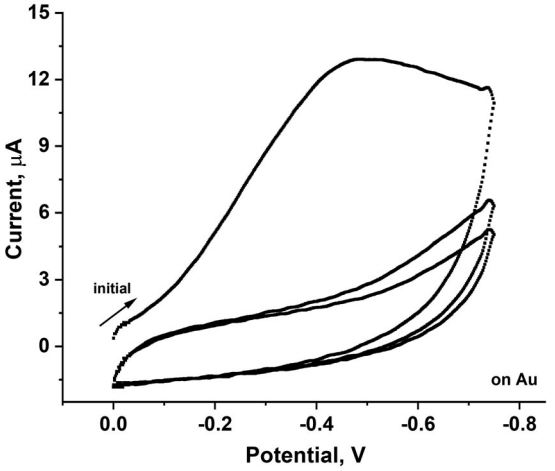

Figure 1. Cyclic voltammograms for three cycles of 36 mM 4-mercaptobenzene and 144 mM $NaNO_2$ in 0.5 M HCl on the Au slide. The reference electrode was $Ag/AgCl/KCl_{sat.}$ and the scan rate was 200 mV/s.

Table 2. Thickness of the 4-MP nanofilm on the gold slide measured by ellipsometry.

Number of cycles	Relative thickness ± standard deviation (nm, $n = 5$)
1	1.247 ± 0.078
2	2.435 ± 0.135
3	2.995 ± 0.184

equilibrium in the second and third cycles. Since the thickness was obtained per model, the thickness values should be considered to be a measure of the deposition of the 4MP nanofilm on the surface but not directly as the monolayer thickness.

Electrochemical characterization of the nanofilm was performed by CV and EIS. A gold disk electrode (BAS, MF-2014, USA) with a 1.6 mm diameter was used instead of a gold nanofilm-coated glass slide. CVs of 1 mM $K_3Fe(CN)_6/K_4Fe(CN)_6$ in 0.1 M KCl on bare Au, 4MP covalently attached gold *via* electrochemical diazonium reduction (Au-4MP), and gold nanoparticle attached Au-4MP (i.e., Au-4MP-AuNP) electrodes and their cathodic current values are shown in Figure 2a, b. Nyquist plots and charge transfer resistance values of the redox couple on the same electrodes are shown in Figure 3a, b.

The electron transfer rate of the redox couple increased for the Au-4MP-AuNP surface in comparison with the other electrodes. This increase in the redox current of the modified surface indicates a higher electron transfer rate and better conductivity. This also may indicate that the surface area improvement after AuNPs immobilization increased the surface area, showing the modification with 4MP-AuNPs.[51] The Nyquist plot was evaluated according to Warburg-effective diffusion-controlled equivalent circuit

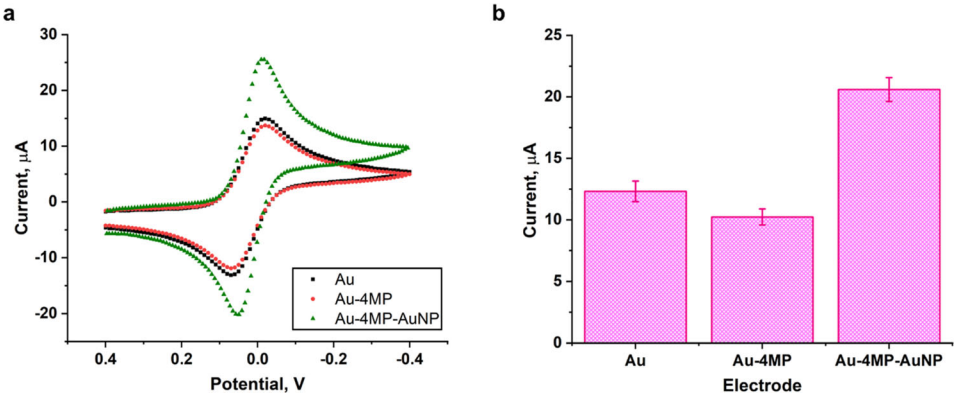

Figure 2. (a) Cyclic voltammograms of 1 mM $K_3Fe(CN)_6/K_4Fe(CN)_6$ in 0.1 M KCl on the bare Au, Au-4MP, and Au-4MP-AuNP electrodes and **(b)** their cathodic current values. The reference electrode was $Ag/AgCl/KCl_{sat.}$ and the scan rate was 200 mV/s.

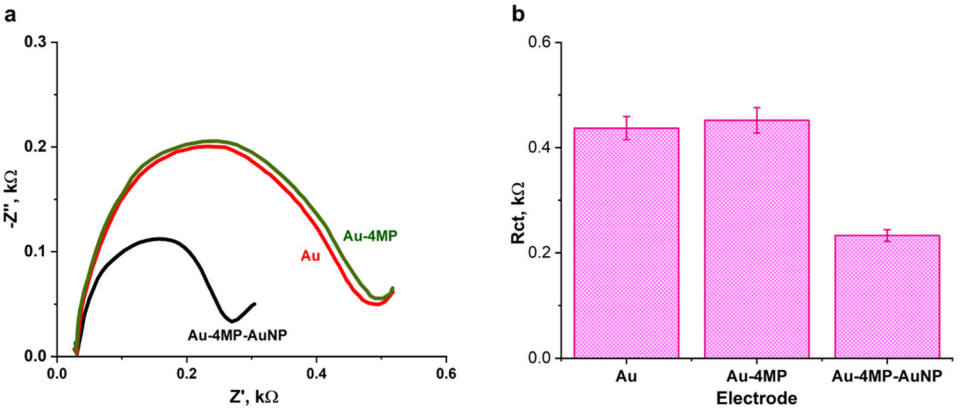

Figure 3. (a) Nyquist plots of 1 mM $K_3Fe(CN)_6/K_4Fe(CN)_6$ in 0.1 M KCl on the bare Au, Au-4MP, and Au-4MP-AuNP electrodes and (b) their charge transfer resistance values. The reference electrode was $Ag/AgCl/KCl_{sat.}$ and the scan rate was 200 mV/s.

modeling.[52] In Figure 3b, the lowest charge transfer resistance of the redox probe was achieved upon the surface of the Au-4MP-AuNP electrode which also agrees with the CV results.

The Au-4MP-AuNP surface was subsequently characterized using XPS. The C 1s spectrum was a broad band at approximately 285 eV in Figure 4a. This band is composed of binding energies at 284.6, 285.6, and 286.1 eV for C 1s corresponding aromatic carbon, C–S, and C–N, respectively.[53] The C aromatic binding energy indicates the presence of the mercaptophenyl structure. The C–S binding energy also indicates the mercapto-functional group on the surface. Both are evidence of 4MP modification. The C–N binding energy corresponds to the residual amine groups (i.e., 4-ATP) from the impurities in MB-DAS used for modification. The S 2p spectra in Figure 4b were fitted and evaluated in terms of $2p^{1/2}$ and $2p^{3/2}$ peaks at

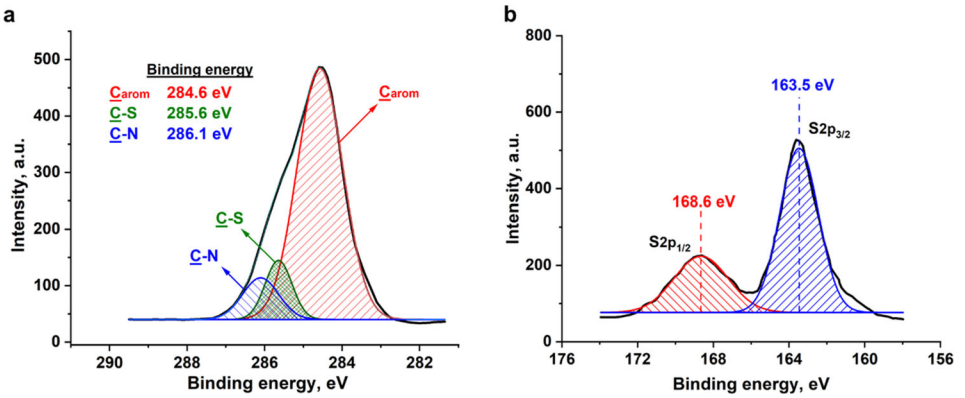

Figure 4. High-resolution X-ray photoelectron spectra of Au-4MP-AuNP. (a) C 1s and (b) S 2p.

163.5 and 168.6 eV, respectively.[54] The split spectra of S 2p also indicates the phenyl-S-Au junction. Therefore, successful surface modification was confirmed by XPS.

For the immobilization of antiCEA1 and antiCEA2 probes, aptamers prepared in PBS at several concentrations were incubated on the surface followed by blocking with mercaptohexanol. The signal was obtained from the sensor using various concentrations of CEA indicating typical surface binding kinetics. Figure S1 was obtained as the average of the signals as the maximum value at the point where equilibrium was reached. Sensor responses obtained with CEA after antiCEA1 (Figure S1a), and antiCEA2 (Figure S1b) immobilization increased depending upon the probe concentration and reached a plateau. Using this response, which is a measure of the aptamer quantity suitable for interaction with CEA as well as the occupancy on the surface, 1.5 µM and 2 h of immobilization were sufficient for the antiCEA1 probe. The optimum immobilization concentration was 2.0 µM for the antiCEA2 probe using the same incubation period.

Sensor calibration was performed using these optimum conditions. CEA solutions from 0.01 to 500 ng/mL were determined by SPRe-TIRE. The response was obtained as the difference of the CEA signal from the PBS blank that demonstrated analyte-ligand binding at the surface for antiCEA1 and antiCEA2 in Figure 5a,b.

A relatively low interaction rate was observed at low CEA concentrations. The responses are similar for both platforms. Plateaus were observed approximately 5 min following injection. The phase shift (Δ) for antiCEA1 was approximately two times higher than for the antiCEA2 probe at the same concentration. However, the lower Δ signals do not necessarily indicate poor analytical performance. In addition, during the surface interaction, the difference in the molecular density of the film on the surface is not a single factor that changes the phase shift, Δ.

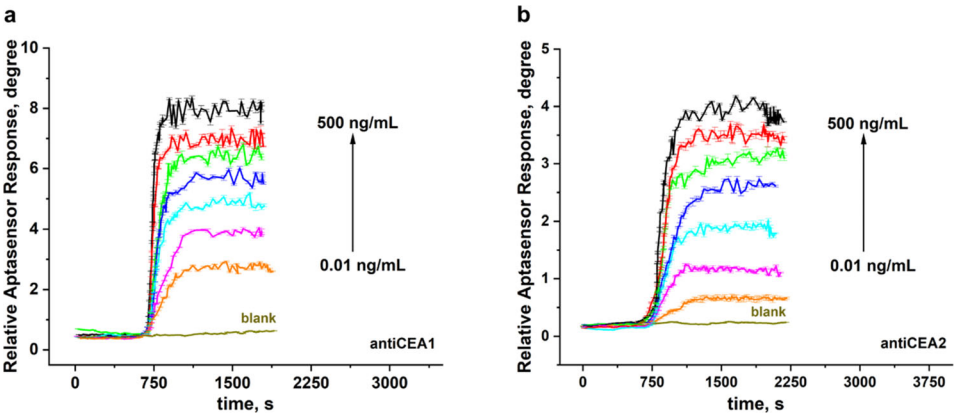

Figure 5. Ellipsometric sensorgrams for several CEA concentrations using the (a) antiCEA1 and (b) antiCEA2 platforms.

Table 3. Calibration relationships for the developed methods ($n = 5$).

	Value	
Analytical feature	AntiCEA1	AntiCEA2
Regression equation	$y = 0.9764x + 4.7766$	$y = 0.6571x + 1.9496$
Standard error of the slope	0.0468	0.0199
Standard error of the intercept	0.0686	0.0359
Coefficient of determination	0.9886	0.9955
Linearity range (ng/mL)	0.01–500	0.01–500
Number of data points	7	7
Limit of detection (pg/mL)	0.1	2.9
Limit of quantification (pg/mL)	0.3	8.7

Similar properties have been observed in our previous work using aptamers for Hg^{2+},[55] in which the film density on the surface did not significantly change after aptamer interaction with the analyte. Hence, although the relative intensity is different for the aptamers, the separation of the signals across the range of CEA concentration is considered to be sufficient. The sensor provided a logarithmic response as expected for an analyte interacting with a limited number of available sites (aptamer probes) on the surface.

The calibration curves for the aptasensors are shown in Figure S2 and are similar except for the magnitude of the response. Both sensor graphs were linear on a semi-log scale ($y = 0.9764x + 4.7766$ for AntiCEA1, $y = 0.6571x + 1.9496$ for AntiCEA2) with a correlation coefficients of 0.9886 and 0.9955, respectively.

The analytical figures of merit are summarized in Table 3. A higher intercept was obtained using the antiCEA1 aptamer due to the intensity of the response (~4.8 Δ, degrees), while it was approximately 1.9 for antiCEA2. The slopes of calibration graphs, which are a measure of the sensitivity, were 0.98 Δ/log [CEA] for antiCEA1, and 0.66 Δ/log [CEA] for antiCEA2, showing the former is more sensitive.

This sensitivity was also characterized by the limits of detection and quantification using the signal-to-noise ratio (S/N). The average standard deviations from the repeated analyses for both sensor platforms were considered to be the noise. The limit of detection (LOD) based upon a signal-to-noise ratio of 3 was 0.1 pg/mL using antiCEA1 probe and 2.9 pg/mL for the antiCEA2 probe. Although there was a 2-fold difference in the relative responses, there was a 30-fold difference in the limits of detection. This result may be due to noise on the platform because of insufficient separation in terms of phase shift (Δ) as a response to CEA interaction at low-concentration levels. This may occur because the antiCEA2probe has lower affinity, as well as the differences in the interaction with the analyte and the length and functional groups of the aptamer sequences. The limit of quantification (LOQ), deemed to be three times the limit of detection, was equal to 0.3 pg/mL and 8.7 pg/mL for antiCEA1 and antiCEA2 probes, respectively.

The precision and accuracy of the SPRe-TIRE platforms using antiCEA1 and antiCEA2 aptamer were characterized and the results are summarized in Table S1. According to the intraday and interday results from samples spiked with 1 and 50 ng/mL CEA, the relative standard deviation and the relative error were below 5%, meeting analytical performance requirements. No bias was obtained based upon the interday and intraday results. The relative standard error was between −5% and +5% for both platforms. The accuracy and precision demonstrate that this platform is suitable for the determination of CEA at low concentrations.

Although the selectivity of aptamers against potential interferences is well known, interference measurements were also performed. All interferents were added at 10-fold excess compared to the CEA analyte (i.e., 50 and 500 ng/mL). The results are summarized in Table 4. The highest interference was obtained from CA125 with a Δ shift of 2.1%. However, all interference values were of comparable magnitude to the precision and accuracy of the sensor. Therefore, there were deemed to be no significant interferences.

To demonstrate practical analysis, 1 and 50 ng/mL CEA was spiked into commercial human serum. Table 5 shows the recoveries were between 95.5 and 104%, meeting the analytical requirements.

Table 4. Influence of interferents at 500 ng/mL on the change of the signal from 50 ng/L CEA using the antiCEA1 probe.

Interferent	Δ signal change upon interferent addition (%)
α-Fetoprotein	+1.4
Cancer antigen-125	+2.1
Vascular endothelial growth factor-165	+1.7

Table 5. Analytical recoveries of the CEA from human serum ($n = 5$) using the antiCEA1 probe.

Sample	Spiked concentration (ng/mL)	Measured concentration of CEA (ng/mL)	Recovery (%)
I	1	1.04 ± 0.02	104
	50	47.75 ± 2.16	95.5
II	1	0.98 ± 0.02	98.0
	50	51.76 ± 1.65	103.5

Table 6. Comparison of the developed CEA aptasensor with the literature.

Method	Calibration range	Limit of detection	Reference
Electrochemical (Amperometric)	1–200 ng/mL	0.5 ng/mL	[56]
Electrochemical (Impedimetric)	0.05 pg/mL–20 ng/mL	0.023 pg/mL	[57]
Electrochemical (Voltammetric)	1–1000 ng/mL	0.517 ng/mL	[58]
Electrochemical (Potentiometric)	0.01–100 ng/mL	7.3 pg/mL	[59]
Colorimetric	0–120 ng/mL	3 ng/mL	[60]
Surface plasmon resonance	1–250 ng/mL	0.3 ng/mL	[61]
Fluorescence	0.4–100 ng/mL	0.316 ng/mL	[62]
Chemiluminescence	0–200 ng/mL	0.58 ng/mL	[28]
LC-based platform	0.05 pg/mL – 50 ng/mL	0.12 pg/mL	[18]
Surface-enhanced Raman scattering	1–50 ng/mL	0.1 ng/mL	[63]
SPRe-TIRE	0.01–500 ng/mL	0.1 pg/mL	This study

Conclusions

Herein, a novel CEA detection platform is reported by adapting two affinity aptamers from the literature. This platform was based on real-time measurements to calculate the phase shift (Δ), an ellipsometric parameter. Another goal was to develop a highly sensitive CEA platform by including the SPR phenomenon in ellipsometry which was achieved. AuNPs were attached to the surface to enhance the signal, with favorable responses for 0.01 ng/mL to 500 ng/mL CEA.

Although the affinities of the two aptamers differ, low limits of detection of 0.1 and 2.9 pg/mL were obtained for the antiCEA1 and antiCEA2 aptamer, respectively. In the interday and intraday measurements, the standard deviation and standard error were below 5%, demonstrating good accuracy and precision. Both aptasensors were demonstrated to be selective for potential interferences with a maximum deviation of less than 3% with a positive bias in sensor response. Spiked human serum was analyzed for CEA with recoveries between 95% and 105%.

Table 6 is a comparison of the analytical performance of the reported approach with the literature. The performance of this approach was generally better than in the previous protocols, providing suitable selectivity, sensitivity, precision, and accuracy. Better performance was also obtained compared to the optical, spectroscopic, and chromatographic strategies.

Ellipsometric measurements have potential in biosensing, especially in health-care applications. However, there are a challenge to be addressed since the technology is new and requires additional investigation. Further

studies of the SPRe-TIRE aptasensor for CEA are planned to implement this platform in clinical applications.

Disclosure statement

The authors declare that they have no conflicts of interest.

Funding

This work was supported by TUBITAK (Scientific and Technological Research Council of Turkey) by project number 122Z678.

References

[1] Crosby, D.; Bhatia, S.; Brindle, K. M.; Coussens, L. M.; Dive, C.; Emberton, M.; Esener, S.; Fitzgerald, R. C.; Gambhir, S. S.; Kuhn, P.; et al. Early Detection of Cancer. *Science* **2022**, *375*, eaay9040. DOI: 10.1126/science.aay9040.

[2] Sarhadi, V. K.; Armengol, G. Molecular Biomarkers in Cancer. *Biomolecules* **2022**, *12*, 1021. DOI: 10.3390/biom12081021.

[3] Broggio, J.; Bannister, N. *Cancer Survival by Stage at Diagnosis for England (Experimental Statistics): Adults Diagnosed 2012, 2013 and 2014 and Followed up to 2015*. London, UK: Dandy Booksellers Limited: **2016**.

[4] Hasanzadeh, M.; Shadjou, N.; Lin, Y.; de la Guardia, M. Nanomaterials for Use in Immunosensing of Carcinoembryonic Antigen (CEA): Recent Advances. *Trends Anal. Chem.* **2017**, *86*, 185–205. DOI: 10.1016/j.trac.2016.11.003.

[5] Wu, Q.; Li, N.; Wang, Y.; Xu, Y.; Wu, J.; Jia, G.; Ji, F.; Fang, X.; Chen, F.; Cui, X. Ultrasensitive and Selective Determination of Carcinoembryonic Antigen Using Multifunctional Ultrathin Amino-Functionalized Ti_3C_2-Mxene Nanosheets. *Anal. Chem.* **2020**, *92*, 3354–3360. DOI: 10.1021/acs.analchem.9b05372.

[6] Altintas, Z.; Uludag, Y.; Gurbuz, Y.; Tothill, I. E. Surface Plasmon Resonance Based Immunosensor for the Detection of the Cancer Biomarker Carcinoembryonic Antigen. *Talanta* **2011**, *86*, 377–383. DOI: 10.1016/j.talanta.2011.09.031.

[7] Hall, C.; Clarke, L.; Pal, A.; Buchwald, P.; Eglinton, T.; Wakeman, C.; Frizelle, F. A. Review of the Role of Carcinoembryonic Antigen in Clinical Practice. *Ann. Coloproctol.* **2019**, *35*, 294–305. DOI: 10.3393/ac.2019.11.13.

[8] Li, N.-L.; Jia, L.-P.; Ma, R.-N.; Jia, W.-L.; Lu, Y.-Y.; Shi, S.-S.; Wang, H.-S. A Novel Sandwiched Electrochemiluminescence Immunosensor for the Detection of Carcinoembryonic Antigen Based on Carbon Quantum Dots and Signal Amplification. *Biosens Bioelectron* **2017**, *89*, 453–460. DOI: 10.1016/j.bios.2016.04.020.

[9] Sun, G.; Lu, J.; Ge, S.; Song, X.; Yu, J.; Yan, M.; Huang, J. Ultrasensitive Electrochemical Immunoassay for Carcinoembryonic Antigen Based on Three-Dimensional Macroporous Gold Nanoparticles/Graphene Composite Platform and Multienzyme Functionalized Nanoporous Silver Label. *Anal. Chim. Acta* **2013**, *775*, 85–92. DOI: 10.1016/j.aca.2013.03.009.

[10] Nicholson, B. D.; Shinkins, B.; Pathiraja, I.; Roberts, N. W.; James, T. J.; Mallett, S.; Perera, R.; Primrose, J. N.; Mant, D. Blood Cea Levels for Detecting Recurrent

Colorectal Cancer. *Cochrane Database Syst. Rev.* **2015**, *2015*, CD011134. DOI: 10.1002/14651858.CD011134.pub2.

[11] Szturmowicz, M.; Tomkowski, W.; Fijalkowska, A.; Sakowicz, A.; Filipecki, S. 1268 Is an Increased Carcinoembryonic Antigen (CEA) Concentration in Pericardial Fluid an Indication of Malignant Pericarditis? *Eur. J. Cancer* **1995**, *31*, S264. DOI: 10.1016/0959-8049(95)96514-E.

[12] Tang, D.; Yuan, R.; Chai, Y. Ultrasensitive Electrochemical Immunosensor for Clinical Immunoassay Using Thionine-Doped Magnetic Gold Nanospheres as Labels and Horseradish Peroxidase as Enhancer. *Anal. Chem.* **2008**, *80*, 1582–1588. DOI: 10.1021/ac702217m.

[13] Dela Rosa, A. M.; Kumakura, M. Trapping Method of Antibodies on Surfaces of Polymerizing Discs for Enzyme Immunoassay. *Anal. Chim. Acta.* **1995**, *312*, 85–94. DOI: 10.1016/0003-2670(95)00167-X.

[14] Qiu, Z.; Shu, J.; Tang, D. Bioresponsive Release System for Visual Fluorescence Detection of Carcinoembryonic Antigen from Mesoporous Silica Nanocontainers Mediated Optical Color on Quantum Dot-Enzyme-Impregnated Paper. *Anal. Chem.* **2017**, *89*, 5152–5160. DOI: 10.1021/acs.analchem.7b00989.

[15] Shen, G.-Y.; Wang, H.; Deng, T.; Shen, G.-L.; Yu, R.-Q. A Novel Piezoelectric Immunosensor for Detection of Carcinoembryonic Antigen. *Talanta* **2005**, *67*, 217–220. DOI: 10.1016/j.talanta.2005.02.020.

[16] Cai, Y.; Li, H.; Li, Y.; Zhao, Y.; Ma, H.; Zhu, B.; Xu, C.; Wei, Q.; Wu, D.; Du, B. Electrochemical Immunoassay for Carcinoembryonic Antigen Based on Signal Amplification Strategy of Nanotubular Mesoporous PdCu Alloy. *Biosens. Bioelectron.* **2012**, *36*, 6–11. DOI: 10.1016/j.bios.2012.02.064.

[17] Darain, F.; Park, S.-U.; Shim, Y.-B. Disposable Amperometric Immunosensor System for Rabbit Igg Using a Conducting Polymer Modified Screen-Printed Electrode. *Biosens Bioelectron* **2003**, *18*, 773–780. DOI: 10.1016/S0956-5663(03)00004-6.

[18] Ren, H.; Jang, C.-H. A Simple Liquid Crystal-Based Aptasensor Using a Hairpin-Shaped Aptamer for the Bare-Eye Detection of Carcinoembryonic Antigen. *BioChip J.* **2019**, *13*, 352–361. DOI: 10.1007/s13206-019-3406-1.

[19] Srivastava, S.; Abraham, P. R.; Mukhopadhyay, S. Aptamers: An Emerging Tool for Diagnosis and Therapeutics in Tuberculosis. *Front Cell Infect. Microbiol.* **2021**, *11*, 656421. DOI: 10.3389/fcimb.2021.656421.

[20] Ciancio, D. R.; Vargas, M. R.; Thiel, W. H.; Bruno, M. A.; Giangrande, P. H.; Mestre, M. B. Aptamers as Diagnostic Tools in Cancer. *Pharmaceuticals* **2018**, *11*, 86. DOI: 10.3390/ph11030086.

[21] Ellington, A. D.; Szostak, J. W. In Vitro Selection of Rna Molecules That Bind Specific Ligands. *Nature* **1990**, *346*, 818–822. DOI: 10.1038/346818a0.

[22] Tuerk, C.; Gold, L. Systematic Evolution of Ligands by Exponential Enrichment: RNA Ligands to Bacteriophage T4 DNA Polymerase. *Science* **1990**, *249*, 505–510. DOI: 10.1126/science.220012.

[23] Thiviyanathan, V.; Gorenstein, D. G. Aptamers and the Next Generation of Diagnostic Reagents. *Proteomics Clin. Appl.* **2012**, *6*, 563–573. DOI: 10.1002/prca.201200042.

[24] Song, K.-M.; Lee, S.; Ban, C. Aptamers and Their Biological Applications. *Sensors (Basel)* **2012**, *12*, 612–631. DOI: 10.3390/s120100612.

[25] Xiang, W.; Lv, Q.; Shi, H.; Xie, B.; Gao, L. Aptamer-Based Biosensor for Detecting Carcinoembryonic Antigen. *Talanta* **2020**, *214*, 120716. DOI: 10.1016/j.talanta.2020.120716.

[26] Ma, C.; Liu, H.; Zhang, L.; Li, H.; Yan, M.; Song, X.; Yu, J. Multiplexed Aptasensor for Simultaneous Detection of Carcinoembryonic Antigen and Mucin-1 Based on Metal Ion Electrochemical Labels and $Ru(NH_3)_6^{3+}$ Electronic Wires. *Biosens. Bioelectron.* **2018**, *99*, 8–13. DOI: 10.1016/j.bios.2017.07.031.

[27] A.-Raji, M.; G.-Zadeh, E.; Amoabediny, G. An Optically-Transparent Aptamer-Based Detection System for Colon Cancer Applications Using Gold Nanoparticles Electrodeposited on Indium Tin Oxide. *Sensors* **2016**, *16*, 1071. DOI: 10.3390/s16071071.

[28] Khang, H.; Cho, K.; Chong, S.; Lee, J. H. All-in-One Dual-Aptasensor Capable of Rapidly Quantifying Carcinoembryonic Antigen. *Biosens. Bioelectron.* **2017**, *90*, 46–52. DOI: 10.1016/j.bios.2016.11.043.

[29] Arwin, H. Ellipsometry on Thin Organic Layers of Biological Interest: Characterization and Applications. *Thin Solid Films* **2000**, *377-378*, 48–56. DOI: 10.1016/S0040-6090(00)01385-7.

[30] Johs, B.; Herzinger, C. M. Quantifying the Accuracy of Ellipsometer Systems. *Phys. Status Solidi (c)* **2008**, *5*, 1031–1035. DOI: 10.1002/pssc.200777755.

[31] Tolmachev, V. A.; Gushchina, E. V.; Nyapshaev, I. A.; Zharova, Y. A. Spectroscopic Ellipsometry Study of Dielectric Functions of Ag Films and Chemically Deposited Layers of Ag Nanoparticles on Silicon. *Thin Solid Films* **2022**, *756*, 139352. DOI: 10.1016/j.tsf.2022.139352.

[32] Arwin, H.; Poksinski, M.; Johansen, K. Enhancement in Ellipsometric Thin Film Sensitivity near Surface Plasmon Resonance Conditions. *Phys. Stat. Sol.* (*a*) **2008**, *205*, 817–820. DOI: 10.1002/pssa.200777899.

[33] Nabok, A.; Tsargorodskaya, A. The Method of Total Internal Reflection Ellipsometry for Thin Film Characterisation and Sensing. *Thin Solid Films* **2008**, *516*, 8993–9001. DOI: 10.1016/j.tsf.2007.11.077.

[34] Caglayan, M. O. Plasmon Resonance-Enhanced Internal Reflection Ellipsometry for the Trace Detection of Mercuric Ion. *Int. J. Environ. Sci. Technol.* **2018**, *15*, 909–914. DOI: 10.1007/s13762-017-1450-8.

[35] de Melo, I. A.; Correa, C. R.; da Silva, C. P.; de Góes, A. M.; Gomes, D. A.; de Andrade, A. S. R. DNA Aptamers Selection for Carcinoembryonic Antigen (CEA). *Bioorg. Med. Chem. Lett.* **2020**, *30*, 127278. DOI: 10.1016/j.bmcl.2020.127278.

[36] Poksinski, M.; Arwin, H. Protein Monolayers Monitored by Internal Reflection Ellipsometry. *Thin Solid Films* **2004**, *455-456*, 716–721. DOI: 10.1016/j.tsf.2004.01.037.

[37] Garcia-Caurel, E.; De Martino, A.; Gaston, J. P.; Yan, L. Application of Spectroscopic Ellipsometry and Mueller Ellipsometry to Optical Characterization. *Appl. Spectrosc.* **2013**, *67*, 1–21. DOI: 10.1366/12-06883.

[38] Arwin, H. Is Ellipsometry Suitable for Sensor Applications? *Sens. Actuators, A* **2001**, *92*, 43–51. DOI: 10.1016/S0924-4247(01)00538-6.

[39] Caglayan, M. O.; Üstündağ, Z. Spectrophotometric Ellipsometry Based Tat-Protein RNA-Aptasensor for HIV-1 Diagnosis. *Spectrochim. Acta A: Mol. Biomol. Spectrosc.* **2020**, *227*, 117748. DOI: 10.1016/j.saa.2019.117748.

[40] Li, K.; Wang, S.; Wang, L.; Yu, H.; Jing, N.; Xue, R.; Wang, Z. Fast and Sensitive Ellipsometry-Based Biosensing. *Sensors* **2018**, *18*, 15. DOI: 10.3390/s18010015.

[41] Caglayan, M. O.; Üstündağ, Z. Saxitoxin Aptasensor Based on Attenuated Internal Reflection Ellipsometry for Seafood. *Toxicon* **2020**, *187*, 255–261. DOI: 10.1016/j.toxicon.2020.09.005.

[42] Bombarová, K.; Chlpík, J.; Cirák, J. Surface Plasmon Resonance Ellipsometry Based Biosensor for the Investigation of Biomolecular Interactions. *Mater. Today: Proc.* **2015**, *2*, 70–76. DOI: 10.1016/j.matpr.2015.04.010.

[43] Çağlayan, M. O.; Sayar, F.; Demirel, G.; Garipcan, B.; Otman, B.; Çelen, B.; Pişkin, E. Stepwise Formation Approach to Improve Ellipsometric Biosensor Response. *Nanomedicine* **2009**, *5*, 152–161. DOI: 10.1016/j.nano.2008.12.006.

[44] Üstündağ, Z.; Çağlayan, M. O.; Güzel, R.; Pişkin, E.; Solak, A. O. A Novel Surface Plasmon Resonance Enhanced Total Internal Reflection Ellipsometric Application: Electrochemically Grafted Isophthalic Acid Nanofilm on Gold Surface. *Analyst* **2011**, *136*, 1464–1471. DOI: 10.1039/C0AN00410C.

[45] Morita, K.; Yamaguchi, A.; Teramae, N. Electrochemical Modification of Benzo-15-Crown-5 Ether on a Glassy Carbon Electrode for Alkali Metal Cation Recognition. *J. Electroanal. Chem.* **2004**, *563*, 249–255. DOI: 10.1016/j.jelechem.2003.09.018.

[46] Huang, H.; Yang, X. Chitosan Mediated Assembly of Gold Nanoparticles Multilayer. *Colloids Surf. A* **2003**, *226*, 77–86. DOI: 10.1016/S0927-7757(03)00382-0.

[47] Nguyen, D. T.; Kim, D.-J.; So, M. G.; Kim, K.-S. Experimental Measurements of Gold Nanoparticle Nucleation and Growth by Citrate Reduction of $HAuCl_4$. *Adv. Powder Technol.* **2010**, *21*, 111–118. DOI: 10.1016/j.apt.2009.11.005.

[48] Wang, Q.-L.; Cui, H.-F.; Du, J.-F.; Lv, Q.-Y.; Song, X. In Silico Post-Selex Screening and Experimental Characterizations for Acquisition of High Affinity DNA Aptamers against Carcinoembryonic Antigen. *RSC Adv.* **2019**, *9*, 6328–6334. DOI: 10.1039/C8RA10163A.

[49] Park, S.; Brown, K. A.; Hamad-Schifferli, K. Changes in Oligonucleotide Conformation on Nanoparticle Surfaces by Modification with Mercaptohexanol. *Nano Lett.* **2004**, *4*, 1925–1929. DOI: 10.1021/nl048920t.

[50] İsbir, A. A.; Solak, A. O.; Üstündağ, Z.; Bilge, S.; Natsagdorj, A.; Kiliç, E.; Kiliç, Z. The Electrochemical Behavior of Some Podands at a Benzo[C]Cinnoline Modified Glassy Carbon Electrode. *Anal. Chim. Acta* **2005**, *547*, 59–63. DOI: 10.1016/j.aca.2005.02.049.

[51] Wu, T.; Zhu, Y.; Song, L.; Chen, Y.; Huang, Y.; Tang, J.; Ma, X.; Wang, H.; Zhang, J.; Lin, D.; Chen, G. Three-Dimensional Gold Nanowires with High Specific Surface Area for Simultaneous Detection of Heavy Metal Ions. *Anal. Methods* **2022**, *14*, 859–868. DOI: 10.1039/D1AY02051J.

[52] Yeter, E. Ç.; Şahin, S.; Caglayan, M. O.; Üstündağ, Z. An Electrochemical Label-Free DNA Impedimetric Sensor with Aunp-Modified Glass Fiber/Carbonaceous Electrode for the Detection of Hiv-1 DNA. *Chem. Zvesti* **2021**, *75*, 77–87. DOI: 10.1007/s11696-020-01280-5.

[53] Güzel, R.; Üstündağ, Z.; Ekşi, H.; Keskin, S.; Taner, B.; Durgun, Z. G.; Turan, A. A. İ.; Solak, A. O. Effect of Au and Au@Ag Core–Shell Nanoparticles on the Sers of Bridging Organic Molecules. *J. Colloid Interface Sci.* **2010**, *351*, 35–42. DOI: 10.1016/j.jcis.2010.07.039.

[54] Ekşi, H.; Üstündağ, Z.; Solak, A.; Güzel, R. Synthesis, Characterization and Application of Silver Nanoparticle-Thiophenol Nanocomposite Film on the Glassy Carbon Surface. *Surf. Interface Anal.* **2013**, *45*, 1821–1829. DOI: 10.1002/sia.5328.

[55] Caglayan, M. O. Mercuric Ion Detection by Plasmon-Enhanced Spectrophotometric Ellipsometer Using Specific Oligonucleotide Probes. *Spectrochim. Acta A: Mol. Biomol. Spectrosc.* **2020**, *241*, 118682. DOI: 10.1016/j.saa.2020.118682.

[56] Shu, H.; Wen, W.; Xiong, H.; Zhang, X.; Wang, S. Novel Electrochemical Aptamer Biosensor Based on Gold Nanoparticles Signal Amplification for the Detection of Carcinoembryonic Antigen. *Electrochem. Commun.* **2013**, *37*, 15–19. DOI: 10.1016/j.elecom.2013.09.018.

[57] Zhou, X.; Guo, S.; Gao, J.; Zhao, J.; Xue, S.; Xu, W. Glucose Oxidase-Initiated Cascade Catalysis for Sensitive Impedimetric Aptasensor Based on Metal-Organic Frameworks Functionalized with Pt Nanoparticles and Hemin/G-Quadruplex as Mimicking Peroxidases. *Biosens. Bioelectron.* **2017**, *98*, 83–90. DOI: 10.1016/j.bios.2017.06.039.

[58] Xiang, J.; Pi, X.; Chen, X.; Xiang, L.; Yang, M.; Ren, H.; Shen, X.; Qi, N.; Deng, C. Integrated Signal Probe Based Aptasensor for Dual-Analyte Detection. *Biosens. Bioelectron.* **2017**, *96*, 268–274. DOI: 10.1016/j.bios.2017.04.039.

[59] Chen, Y.; Li, B.; Lyu, P.; Kwok, H. F.; Ge, L.; Wu, Q. Boronate Ester Bond–Based Potentiometric Aptasensor for Screening Carcinoembryonic Antigen-Glycoprotein Using Nanometer-Sized $CaCO_3$ with Ion-Selective Electrode. *Anal. Bioanal. Chem.* **2021**, *413*, 1073–1080. DOI: 10.1007/s00216-020-03067-9.

[60] Luo, C.; Wen, W.; Lin, F.; Zhang, X.; Gu, H.; Wang, S. Simplified Aptamer-Based Colorimetric Method Using Unmodified Gold Nanoparticles for the Detection of Carcinoma Embryonic Antigen. *RSC Adv.* **2015**, *5*, 10994–10999. DOI: 10.1039/C4RA14833A.

[61] Guo, C.; Su, F.; Song, Y.; Hu, B.; Wang, M.; He, L.; Peng, D.; Zhang, Z. Aptamer-Templated Silver Nanoclusters Embedded in Zirconium Metal–Organic Framework for Bifunctional Electrochemical and Spr Aptasensors toward Carcinoembryonic Antigen. *ACS Appl. Mater. Interfaces* **2017**, *9*, 41188–41199. DOI: 10.1021/acsami.7b14952.

[62] Bao, B.; Su, P.; Zhu, J.; Chen, J.; Xu, Y.; Gu, B.; Liu, Y.; Wang, L. Rapid Aptasensor Capable of Simply Detect Tumor Markers Based on Conjugated Polyelectrolytes. *Talanta* **2018**, *190*, 204–209. DOI: 10.1016/j.talanta.2018.07.072.

[63] Lin, Y.; Xu, G.; Wei, F.; Zhang, A.; Yang, J.; Hu, Q. Detection of Cea in Human Serum Using Surface-Enhanced Raman Spectroscopy Coupled with Antibody-Modified Au and γ-Fe_2O_3@Au Nanoparticles. *J. Pharm. Biomed. Anal.* **2016**, *121*, 135–140. DOI: 10.1016/j.jpba.2016.01.027.